galaxies

MDPI

Article

An Array of Bulk Acoustic Wave Sensors as a High-Frequency Antenna for Gravitational Waves

Giorgia Albani [1,2], Matteo Borghesi [1,2], Lucia Canonica [1,2,*], Rodolfo Carobene [1,2], Federico De Guio [1,2], Marco Faverzani [1,2], Elena Ferri [2], Raffaele Gerosa [1,2], Alessio Ghezzi [1,2], Andrea Giachero [1,2], Claudio Gotti [2], Danilo Labranca [1,2], Leonardo Mariani [1], Angelo Nucciotti [1,2], Gianluigi Pessina [2], Davide Rozza [1,2] and Tommaso Tabarelli de Fatis [1,2,*]

[1] Dipartimento di Fisica, Università degli Studi di Milano Bicocca , Piazza della Scienza 3, 20126 Milan, Italy; giorgia.albani@unimib.it (G.A.); matteo.borghesi@unimib.it (M.B.); rodolfo.carobene@unimib.it (R.C.); federico.deguio@unimib.it (F.D.G.); marco.faverzani@unimib.it (M.F.); raffaele.gerosa@unimib.it (R.G.); alessio.ghezzi@unimib.it (A.G.); andrea.giachero@unimib.it (A.G.); danilo.labranca@unimib.it (D.L.); l.mariani48@campus.unimib.it (L.M.); angelo.nucciotti@unimib.it (A.N.); davide.rozza@unimib.it (D.R.)

[2] Istituto Nazionale di Fisica Nucleare, Sezione di Milano-Bicocca, Piazza della Scienza 3, 20126 Milan, Italy; elena.ferri@mib.infn.it (E.F.); claudio.gotti@mib.infn.it (C.G.); gianluigi.pessina@mib.infn.it (G.P.)

* Correspondence: lucia.canonica@unimib.it (L.C.); tommaso.tabarelli@unimib.it (T.T.d.F.)

Abstract

In their simplest form, bulk acoustic wave (BAW) devices consist of a piezoelectric crystal between two electrodes that transduce the material's vibrations into electrical signals. They are adopted in frequency control and metrology, with well-established standards at frequencies of 5 MHz and above. Their use as a resonant-mass strain antenna for high-frequency gravitational waves has been recently proposed (Goryachev and Tobar, 2014). The estimated power spectral density sensitivity at the resonant frequencies is of the order of 10^{-21} strain$/\sqrt{\text{Hz}}$. In this paper, after introducing the science opportunity and potential of gravitational wave detection with BAWs, we describe the two-stage BAUSCIA project plan to build a multimode antenna based on commercial BAWs, followed by an optimized array of custom BAWs. We show that commercially available BAWs already provide sensitivity comparable to current experiments around 10 MHz. Finally, we outline options for optimization of custom devices to improve sensitivity in an unexplored region, probe multiple frequencies between 0.1 and 10 MHz, and target specific signals, such as post-merger emission from neutron stars or emission from various dark matter candidates.

Keywords: gravitational waves; resonant-mass strain antenna; acoustic cavities

Academic Editor: Lorenzo Iorio

Received: 10 June 2025
Revised: 8 August 2025
Accepted: 11 August 2025
Published: 15 August 2025

Citation: Albani, G.; Borghesi, M.; Canonica, L.; Carobene, R.; De Guio, F.; Faverzani, M.; Ferri, E.; Gerosa, R.; Ghezzi, A.; Giachero, A.; et al. An Array of Bulk Acoustic Wave Sensors as a High-Frequency Antenna for Gravitational Waves. *Galaxies* **2025**, *13*, 94. https://doi.org/10.3390/galaxies13040094

1. Introduction

The direct observation of gravitational waves (GWs) by interferometric experiments [1] marked the beginning of a new era of astrophysical investigation, which makes it possible to test gravitation and set new constraints on astrophysical models. The search for correlations between gravitational and electromagnetic signals has promptly become a new standard that enabled, for example, the first measurement of the expansion parameter of the universe using gravity alone [2]. Current and future interferometers, on the ground or in space, will mark a significant step forward in studying gravitational waves. The expected sensitivity of planned large-scale projects [3] will consolidate the knowledge of massive and supermassive GW sources and expand the observable horizon into the high-redshift

deep past. However, these projects only target gravitational signals at frequencies lower than approximately 1 kHz, with a cut-off essentially set by the length scale of the apparatus.

Theoretical motivations for potential sources of high-frequency gravitational waves (HFGWs) have been steadily increasing recently [4]. In the region between 0.1 and 10 MHz, corresponding to the sensitivity of the experimental technique discussed in this paper, notable examples include GW emission from dark matter candidates, like mergers of planetary-mass primordial-black-hole binaries [5] or axions collapsing into a massive black hole [6], and from conventional processes, like QCD phase transitions following the event merger of neutron-star binaries [7]. Therefore, an apparatus with sensitivity in this frequency range is well motivated. It would be both complementary and supplementary to large-scale interferometers: GW detection in this range would indicate the existence of non-conventional sources or confirm the observation of neutron-star mergers in coincidence with GW interferometers.

In parallel with the growth of theoretical motivations, many experimental methods have been explored and shown to exhibit sensitivity to HFGWs at different frequencies, from 100 kHz to above 1 GHz. These include small-scale interferometers [8–12], dissimilar techniques exploiting the coupling between gravitational and electromagnetic fields [13–19], gravitational shifts of the Mössbauer absorption [20], and various resonant-mass detectors [21–24]. Bulk-acoustic wave (BAW) devices belong to the latter category. They consist of a piezoelectric crystal between two electrodes that converts the acoustic waves within the material into electrical signals. They are adopted in frequency control and metrology, with well-established standards at frequencies of 5 MHz and above, and give one of the best levels of frequency stability, with Q-factors of the order of 10^6 at room temperature.

Following a seminal paper by Goryachev and Tobar [23], the use of BAWs as a resonant-mass strain antenna has been developed and successfully brought into operation at the University of Western Australia (UWA) [25,26]. For GW detection, BAWs act as acoustic resonant cavities with high sensitivity to impinging strain fields with frequencies matched to the cavity vibration modes. The electric signals generated by crystal vibrations are read out by a superconducting quantum interference device (SQUID) amplifier coupled to the quartz resonator electrodes. The system operates at cryogenic temperatures ($T < 4$ K), where the thermal noise is reduced and the Q-factor of the cavities increases. The latest setup, dubbed Multimode Acoustic Gravitational Wave Experiment (MAGE) [26], features two identical BVA-type quartz resonators [27] coupled to two independent SQUID amplifiers held at a constant temperature of 4 K. Each detector is sensitive to gravitational radiation in multiple narrow bands corresponding to the crystal's overtone modes between 5 and 10 MHz, which are simultaneously monitored. The projected peak spectral strain sensitivity, expressed in terms of single-sided power spectral density, for operation at 20 mK is 5–10 $\times$ 10^{-22} strain/$\sqrt{\text{Hz}}$.

This paper describes the BAUSCIA project (Milan's transliteration of BAWSHA for bulk acoustic wave sensors for high-frequency antennas). In a two-stage plan, we aim to build a multimode antenna based on commercial BAWs for multi-site detection in coincidence with MAGE, followed by an optimized array of BAWs to sample multiple frequencies between 100 kHz and 10 MHz. After a description of the experimental approach (Section 2), we discuss the characterization of some commercially available devices, which turn out to be suitable for an antenna with sensitivity and frequency coverage comparable to MAGE (Section 3). Dedicated effort into research and development will improve the sensitivity and extend coverage to frequencies beyond those of direct interest to commercial applications (Section 4). For illustration, Figure 1 compares the signal strength of putative GW sources with the envelope of the projected single-sided peak strain sensitivities of an

array of tens of BAWs, estimated in Section 4. The figure also shows the complementarity of high-frequency GW detectors to the existing or planned large-scale interferometers, which cover a disjoint frequency interval.

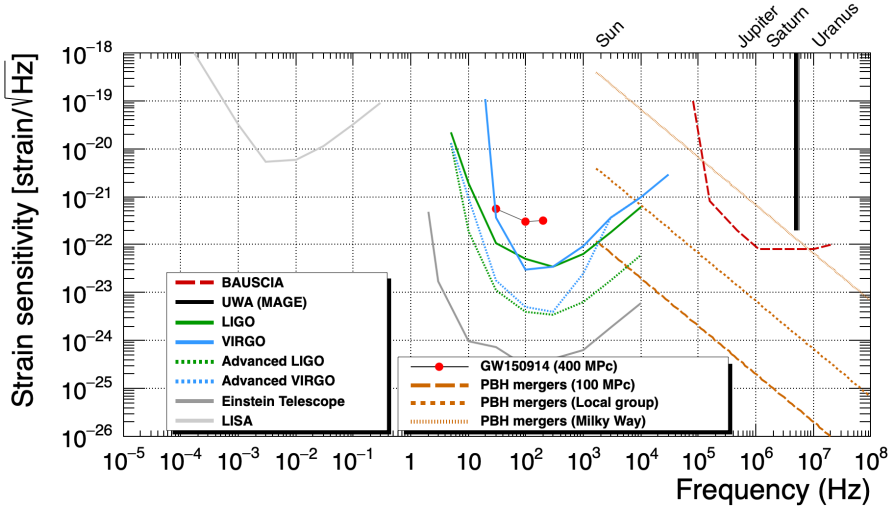

Figure 1. Sensitivity of a current BAW antenna (black line) [26] and potential coverage of the proposed array of BAWs (red line) compared to the sensitivity of existing and planned interferometers (adapted from Ref. [3]) and putative GW radiation from planetary-mass primary-black-hole mergers.

In addition to high-frequency gravitational waves, this apparatus can probe various dark matter scenarios, including ultralight scalars [28,29] or dark photons [30]. The sensitivity depends approximately on the same BAW parameters as for GW searches. Bulky piezoelectric crystals with resonant frequencies in the 10–100 kHz range could evade current constraints.

2. Materials and Methods

The instrumental technique adopted by the BAUSCIA project is based on the pioneering work that led to the MAGE. A key objective of BAUSCIA is the construction of an apparatus with sensitivity across more than two decades of frequencies to offset the narrow-band response limitation of the resonant-cavity approach to GW detection. To this end, the apparatus is designed for scalability. The left panel of Figure 2 sketches the baseline modular structure and the readout chain of the prototype under development. Each module features four BAW sensors coupled to independent SQUID amplifiers, matching the modularity of the prototype back-end system. An external veto against cosmic rays will be considered to exclude potential sources of spurious events, as those observed in [25]. Spurious signals from relaxations of internal crystal stresses can be suppressed by requiring the coincidence of multiple BAWs.

An impinging gravitational wave causes a driving force on the BAW mass elements proportional to the Riemann tensor perturbation from the wave: $(d^2x^j/dt^2) = (R^j_{0k0})x^k$. For a GW-driven resonator, the equation of motion for the displacement $u_\lambda(\mathbf{x}, t) = a_\lambda(t)U_\lambda(\mathbf{x})$ of a stationary mode λ reads as follows:

$$\ddot{a}_\lambda + \gamma_\lambda \dot{a}_\lambda + \omega_\lambda^2 a_\lambda = -c^2 R_{0i0j} \int_V \frac{\rho}{m_\lambda} U^i_\lambda(\mathbf{x}) x^j dv \tag{1}$$

where γ_λ and $\omega_\lambda = 2\pi f_\lambda$ are the mode width and angular frequency, ρ is the mass density of the BAW, and $m_\lambda = \int_V U^2_\lambda \rho dv$ is its effective mass or, in other words, the mass that participates in the vibration. The integral over the BAW volume on the right-hand side of Equation (1) quantifies the coupling between the impinging GW and the acoustic mode of the cavity [23].

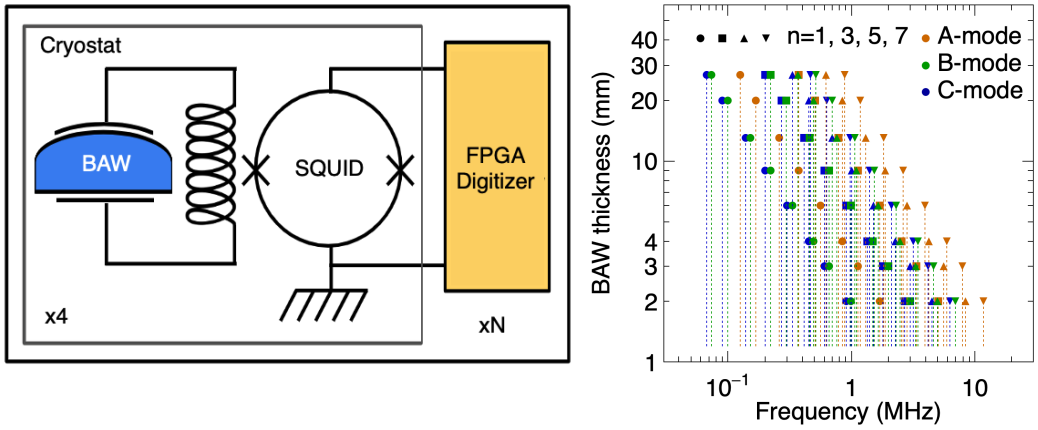

Figure 2. Sketch of the BAUSCIA module prototype (left panel) and map of the resonant frequencies of an array of eight quartz BAWs of different thicknesses (right panel): A, B, and C identify the longitudinal, fast, and slow shear acoustic modes, and n is the overtone number (see text for details).

Quartz cavities support vibrations with longitudinal (A mode) and transverse polarizations (fast and slow shear or B and C modes), with different phase velocities that depend on the orientation of the crystal cut [31]. The crystal thickness and the phase velocities set the frequency spectrum of the modes. Only odd overtones exhibit a piezoelectric counterpart that gives rise to a voltage difference between the top and bottom electrodes, yielding a rich spectrum of audible resonant frequencies:

$$f_{n,X} = n\frac{v_X}{2d}, \quad (n = 1,3,5,\ldots; X = A,B,C) \tag{2}$$

This combination of modes and overtones allows a single BAW to sample multiple frequencies over a broad range. All the BAWs of the current prototype have a thickness $d = 1$ mm (Section 3). They are doubly rotated stress-compensated (SC) cut plates [32], realized from high-purity crystal quartz and optimized for clock applications at $f \simeq 5$ MHz, corresponding to the third overtone of the slow-shear C-mode. In SC-cut plates, the phase velocities are $v_A = 6757$ m/s (A-mode), $v_B = 3966$ m/s (B-mode), and $v_C = 3611$ m/s (C-mode). An array of BAWs of different thicknesses will enable sampling a broader spectrum of frequencies, as illustrated in the right panel of Figure 2.

The signal from the BAW resonators is read out using DC-SQUIDs with a nominal input impedance of 400 nH and 20/50 MHz FLL/open-loop bandwidth[1]. The BAW sensors and the readout SQUID amplifier are operated at cryogenic temperature, in a dilution refrigerator that can reach a base temperature of 20 mK. The back-end data acquisition, outside the dilution refrigerator, adopts field programmable gate array (FPGA) waveform digitizers[2] to continuously and simultaneously monitor all the relevant resonant modes on a single readout line through digital lock-in amplification. This system provides the flexibility to adapt to hardware changes, chiefly the BAW thickness and corresponding resonant frequencies. For scalability, we also consider an alternative layout with multiple (two or four) BAWs in parallel at the input of a single SQUID, to overcome the inadequate availability of SQUIDs on the market. Based on previous work [23,26], we expect the sensitivity of each independent readout line to be limited by the BAW thermal noise at resonance. Multiple BAWs with narrow resonances at different frequencies on the same readout line would remain electrically and mechanically decoupled (except for a change in the input impedance to the SQUID) and only add off-resonance, damped noise. The results of this layout will be the subject of a future report.

The peak sensitivity at the resonant frequencies is described by the single-sided power spectral density of the Nyquist thermal noise produced by the quartz resonator near an acoustic mode [23,26]:

$$S_h^+(\omega_\lambda) = \frac{2}{\bar{\xi}_\lambda d}\sqrt{\frac{k_b T_\lambda}{m_\lambda Q_\lambda\, {\omega_\lambda}^3}} \quad [\text{strain}/\sqrt{\text{Hz}}], \tag{3}$$

where k_b is the Boltzmann constant, and T_λ, m_λ, and Q_λ are the mode temperature, effective mass, and quality factor. The term $\bar{\xi}_\lambda d/2$, where d is the BAW thickness, is a shorthand notation for the integral on the right-hand side of Equation (1), which expresses the coupling between the impinging GW and the acoustic mode of the cavity. The unit-less coupling parameter $\bar{\xi}_\lambda$ is inversely proportional to the square of the overtone number ($\bar{\xi}_\lambda \propto 1/n^2$) through a coefficient of the order of 1, which accounts for the trapping of the vibrational energy within the BAW volume [23]. For well-trapped modes, the effective mass scales as $m_\lambda \propto 1/n$ (see next section). As a consequence, net of quality factor variations with the overtone, the noise power spectral density increases with the overtone as $S_h^+(\omega_\lambda) \propto n$. In other words, a given cavity provides optimal sensitivity at the lowest overtones of its resonant modes ($n \lesssim 7$). Figures of merit of a BAW-based antenna at a resonant frequency are a low operating temperature (cryogenic), a high effective mass, and a large quality factor. All the relevant parameters depend on the BAW geometry and the operating temperature and must be characterized experimentally.

3. Results on Bulk Acoustic Wave Cavities

A bulk acoustic wave cavity consists of a plate of piezoelectric material specially designed to support acoustic vibrations with high quality factors. Ideally, the vibrating part of the plate is mechanically isolated from the environment to minimize any energy leakage. A typical realization is a thin disk of radius L and thickness $d \ll L$ with plano-convex surfaces, anchored by rigid clamps from the sides. The surface curvature traps the vibrations in the centre of the cavity, reducing the dissipation through the clamps [33,34]. For effective excitation and pick-up of the vibrations, the plate is sandwiched between two electrodes, either deposited on the surface or separated from it by a thin vacuum gap. The latter configuration, known as BVA [27], further isolates the vibrating mass from the environment. Figure 3 shows a schematic cross-section of half the radial extension and the transverse distribution of trapped phonons for some acoustic modes, for the two sets of BAW samples characterized in this work. Their geometries are compared in Table 1.

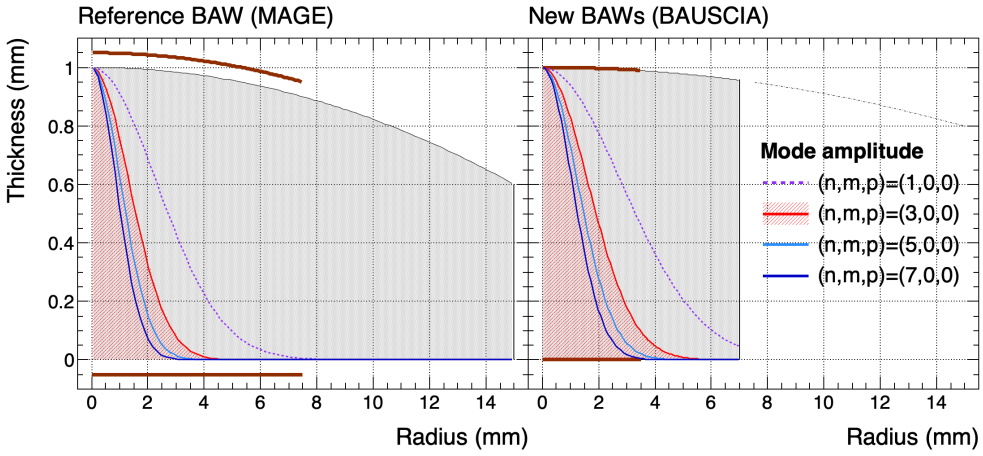

Figure 3. Cross-section in the (z, r) plane of half the radial extension of the reference (**left**) and new (**right**) bulk acoustic wave samples (gray shade) with readout electrodes (bold lines). The lines show the amplitude profile of the modes in the transverse plane for $\lambda = \{X, n, 0, 0\}$ (see text for details).

Table 1. Properties of the reference and new BAW cavities: thickness, d; radius, L; radius of curvature of the convex surface, R_c; and effective radius of the phonon distribution, σ_1, for the overtone number $n = 1$ (see text for details).

Sample	d (mm)	L (mm)	R_c (mm)	σ_1 (mm)	Electrode
Reference	1	15	300	2.3	separated
New	1	7	600	2.8	deposited

The reference sample (courtesy of M. Tobar and collaborators) is identical to the BAWs used in the MAGE. It consists of a 1 mm thick, 30 mm diameter, electrode-separated SC-cut disk, manufactured by Oscilloquartz SA [34], which is no longer in production. The new samples are 1 mm thick and 14 mm diameter SC-cut disks, with 7 mm diameter and 200 nm thick gold electrodes deposited on the disk surfaces (Figure 4), from the Rakon Ltd catalogue[3]. All the resonators, enclosed in a vacuum-tight case, provide Q-factors between 1 and 2×10^6 at room temperature.

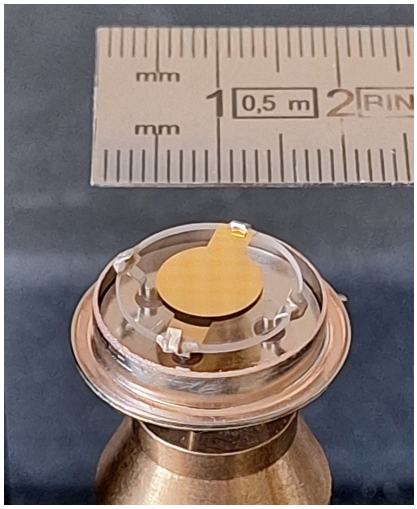

Figure 4. Picture of a 1 mm thick, 14 mm diameter BAW sample made by a plano-convex quartz crystal anchored by four clamps and thin gold electrodes deposited on the surfaces (printed with permission from Rakon Ltd.).

The curvature radius is smaller in the reference ($R_c = 300$ mm) than in the new samples ($R_c = 600$ mm). Consequently, the trapping of the acoustic modes is less pronounced in the new samples, and the vibrations extend closer to the edges of the crystals. However, as illustrated in Figure 3, the main modes are well trapped in both geometries for $n \geq 3$. The mode amplitudes have 2D-normal profiles of comparable radial width, $\sigma_n = \left(d^3 R_c\right)^{1/4} / \sqrt{\pi n}$ (~2.5 mm for $n = 1$), and the effective mass, given by the integral over the crystal volume of the amplitude profile times density.

These profiles are derived under the approximation of an isotropic crystal lattice and a cavity with thickness $d = d(x, y)$, slowly varying as a function of the radial coordinate [33,35]. The surface curvature effectively acts as a two-dimensional harmonic potential because of the inverse proportionality between the frequency (phonon energy) and the local plate thickness. The maximum thickness determines the frequency of the main modes, as specified by Equation (2). In addition, the plano-convex geometry admits thickness modes with polynomial-normal amplitude profiles. In this case, the amplitude maximum is off the disk centre. Consequently, these modes are frequency-shifted relative to the main modes:

$$f_\lambda \sim n f_{\{X,1,0,0\}} + \frac{n-1}{2}(\Delta f_x + \Delta f_y) + m\Delta f_x + p\Delta f_y, \quad (4)$$

where $\lambda = \{X, n, m, p\}$ identifies the mode, through its polarization, overtone number, and two additional integer numbers, m and p, that characterize the mode amplitude in (x, y). The frequency shifts Δf_x and Δf_y depend on the crystal properties and curvature, and their measurement quantifies the trapping in the x and y directions [35]. The parameterization includes two directions because the crystal lattice is not symmetric around the vertical axis. These modes are more spread in the transverse plane, less trapped than the main modes ($m = p = 0$), and generally result in lower Q-factors.

The resonator characterization relies on impedance measurements as a function of frequency performed through a vector network analyzer (VNA). For example, the VNA can be coupled to the resonator in a reflection geometry, with one electrode connected to one port and the other to ground. The coupling coefficient $\beta_\lambda = R_\lambda / R_{\mathrm{VNA}}$ can be extracted from the values of the scattering parameters on resonance, where R_λ is the motional resistance of the mode, and $R_{\mathrm{VNA}} = 50\ \Omega$ is the output impedance of the VNA. A typical resonance scan is shown in the left panel of Figure 5. The quality factor extracted from the full width at half maximum of the resonance curve, $Q_{\lambda,L} = f_\lambda / \Delta f$, includes both resonator losses and those due to coupling with the VNA transmission line ('loading' effect). The quality factors of the resonator ('unloaded') are derived from the unfolding of the coupling coefficient $Q_{\lambda,u} = (1 + \beta_\lambda) Q_{\lambda,L}$.

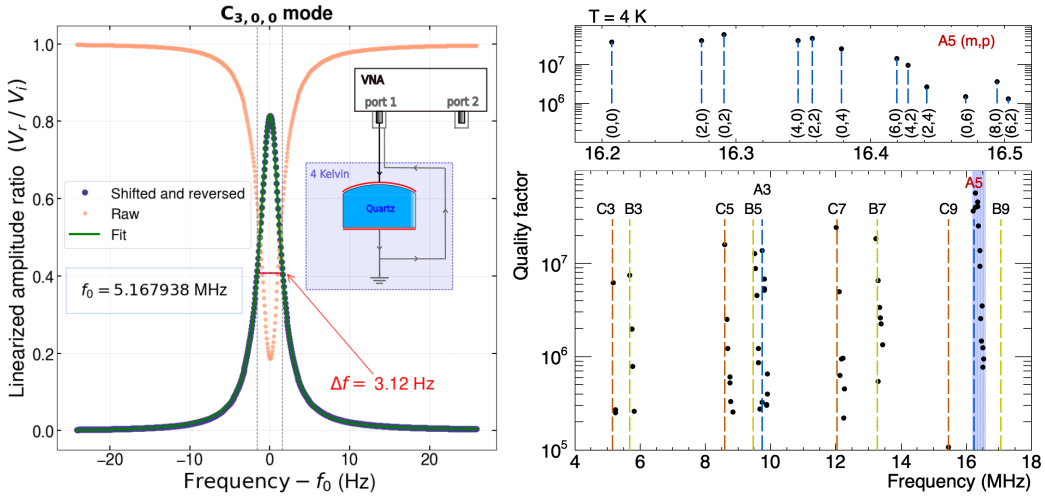

Figure 5. Left: Frequency scan around the resonance for the mode $\lambda = \{C, 3, 0, 0\}$ at $T = 3.5$ K. The inset shows the connection to the VNA. **Right**: Identified resonant modes for one BAW sample at $T = 4$ K as a function of the frequency: the main modes ($m = p = 0$) are marked with vertical lines; the top panel shows the frequency pattern of thickness transverse modes for $\lambda = \{A, 5, m, p\}$.

The unloaded Q_λ factors of the resonances observed between 5 and 20 MHz at $T = 3.5$ K with one of the new samples are displayed in the right panel of Figure 5. Families with overtone numbers $n = 3$, 5, and 7 are well visible for the longitudinal, fast, and slow shear modes. The resonant frequencies are approximately 0.15% lower than at room temperature, indicating a slight variation in the phase velocity with temperature. For all the main modes ($m = p = 0$), the Q-factors at low temperature are over 10^7, and reach 3.5×10^7 for the fifth overtone of the longitudinal mode, $\lambda = \{A, 5, 0, 0\}$. Within a family, the Q-factors decrease with increasing frequency, indicating that for $(m, p) \neq (0, 0)$, the modes are less trapped as predicted. The inset in the figure shows a magnification of the frequency pattern for $\lambda = \{A, 5, m, p\}$. Only modes with even m and p exhibit a piezoelectric counterpart.

The gain in performance at low temperature is remarkable and comparable to the reference and MAGE resonators [26]. To gain insight into loss mechanisms in our samples, we studied the temperature dependence of the cavity losses. Temperature-dependent

intrinsic losses, $1/Q_T$, and mechanical losses, such as the lack of trapping or losses through the electrodes, $1/Q_m$, contribute to the total loss, $1/Q = 1/Q_T + 1/Q_m$. Results are shown in the left panel of Figure 6 for a few representative modes with $m = p = 0$ for both the reference and the new samples. The longitudinal modes benefit most from low-temperature operation. The losses follow a power law with index $\gamma \gtrsim 3$ down to $T \sim 7$ K. At a lower temperature, the losses show a milder scaling as $\propto T^{1/3}$. These behaviours agree with previous studies on BAWs, including the reference sample of this study [34,36]. The main loss mechanism is attributed to the scattering of acoustic waves off thermal phonons. The gentler low-temperature dependence is linked to phonon interactions with two-level systems related to ionic impurities within the crystal. From $T \sim 3$ K to ~ 20 mK, the Q-factors of the new samples improve only marginally, suggesting that in this regime the performance is limited by mechanical losses.

Thermal losses in acoustic resonators have a complex dependency on frequency and temperature, contingent on the relationship between thermal and acoustic phonon energies. For the main modes at low overtones, the loss versus frequency follows approximately a power law, with power indices 0.8 and -1.2 at room temperature and $T = 4$ K, respectively (right panel of Figure 6). Not all modes are observed above 16 MHz ($A5$), and trends become less clear. Residual mechanical losses through the clamps and electrodes may explain the observed pattern [34,36]. Yet, resonators with the electrodes deposited on the crystal have a simple design and are easier to realise than electrode-separated devices. They represent a good choice for future developments, as they already provide excellent performance on the modes with significant coupling to gravitational waves.

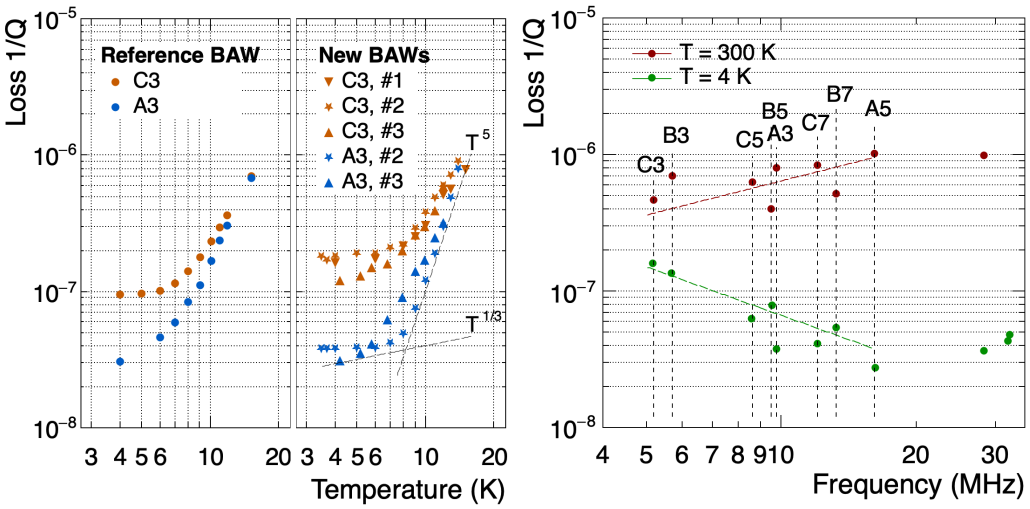

Figure 6. Left: Dependence of the resonator losses on temperature for the modes with $\lambda = \{X, 3, 0, 0\}$; the dashed lines represent the two-level-system loss regime ($T^{1/3}$), and higher-order scaling regimes (T^5), ascribed to phonon–phonon scattering. **Right**: Measurements of $1/Q$ as a function of the frequency for the observed main modes $\lambda = \{X, n, 0, 0\}$ ($n = 3, 5, 7$) at $T = 4$ and 300 K; the dashed lines are empirical power laws through the points with indices 0.8 and -1.2, respectively.

4. Discussion: Antenna Sensitivity and Optimizations

The new BAW samples are an excellent choice for constructing a prototype antenna designed to detect high-frequency gravitational waves. The effective mass of these samples is comparable to that of the reference sample, despite their smaller transverse size. Additionally, the surface curvature effectively traps the main acoustic modes, and the electrode deposition on the plates does not significantly impact the performance, resulting in observed Q-factors exceeding 10^7. Within the frequency range of 5 to 20 MHz, these resonators exhibit strain sensitivity comparable to that of the MAGE.

The results of our characterization are summarized in Figure 7, showing the single-sided peak spectral strain sensitivity derived from Equation (3) for multiple BAW modes and different devices at $T = 3.5$ K. The new BAW samples (full dots) and the MAGE reference sample (open dots) provide comparable single-sensor peak strain sensitivities around 1–3 $\times 10^{-20}$ strain$/\sqrt{\text{Hz}}$. The sensitivities are scaled from the sensitivity reported by the MAGE [26], based on the Q_λ measurements, the effective mass, and the phonon trapping described in this paper. The mode temperatures, T_λ, are assumed equal to the operating temperature, because the characterization of the readout chain and calibration of the SQUIDs are still in progress.

The figure also shows the single-sensor sensitivity predicted for operation of the same BAW samples at $T = 20$ mK (squares). The thermal noise reduction results in a tenfold increase in sensitivity, achieving values around or below 10^{-21} strain$/\sqrt{\text{Hz}}$, despite Q-factors not showing significant improvement below 3.5 K.

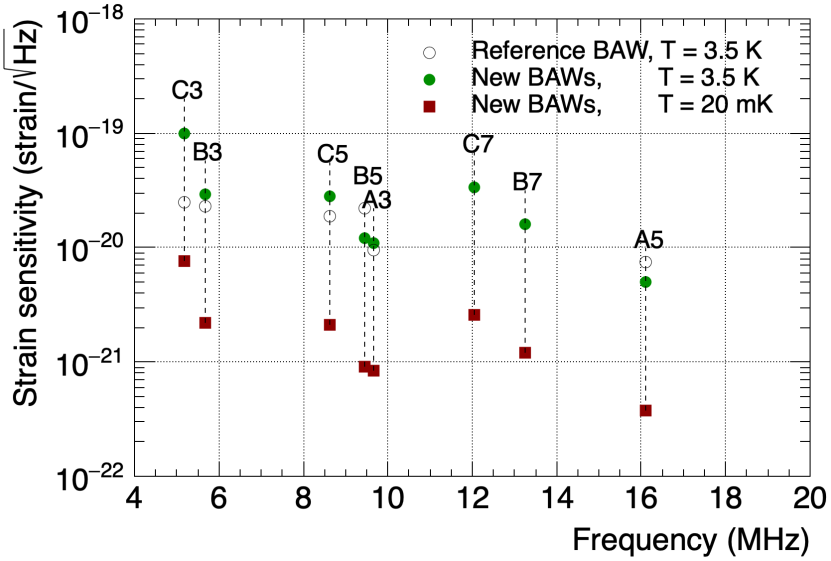

Figure 7. Predicted single-sensor peak spectral strain sensitivity for multiple modes at $T = 3.5$ K for the reference (empty dots) and the new samples (full dots), and for the new samples at $T = 20$ mK (squares).

Commercially available resonators only provide specific frequencies related to telecommunication or clock standards. Additionally, efforts toward miniaturization shift the reference standards to higher frequencies, resulting in reduced coupling to the incoming gravitational waves due to the lower mass of the resonator. Consequently, custom BAWs are being developed to enhance the sensitivity and extend the frequency coverage at low frequencies. Assuming complete trapping of the phonons by proper disk shaping, considering the proportionality of the effective mass with the crystal density ρ and volume $\pi L^2 d$, and expressing the frequency according to Equation (2), the peak strain sensitivity of Equation (3) scales as follows:

$$S_h^+(\omega_\lambda) \propto \frac{n}{L}\sqrt{\frac{k_b T_\lambda}{\rho Q_\lambda v^3}} \quad [\text{strain}/\sqrt{\text{Hz}}]. \tag{5}$$

Optimized performance requires a large radius, which impacts the resonator mass, a fast crystal, and low overtone numbers. Instead, the crystal thickness determines the BAW frequency spectrum but does not directly influence sensitivity, which depends on frequency solely through the overtone number. Therefore, a broad frequency coverage while maintaining consistent sensitivity requires several BAW devices with varying thicknesses.

The sensitivity in Equation (5) does not have any explicit dependence on the piezoelectric coefficient of the BAWs. Different cuts or crystal choices result in different efficiencies for the mechanical-to-electrical energy conversion. However, it does not affect the peak strain sensitivity because it amplifies both the signal and noise from thermal fluctuations. The possibility of enhanced coupling of the quadrupole GW signal for specific symmetries of the crystal lattice, suggested in recent literature [37], is not considered in this paper.

For the project's second phase, we are developing high-purity quartz BAWs of eight different thicknesses varying from 2 to 27 mm, as illustrated in Figure 2. We are working closely with manufacturers to address several aspects of crystal customization, including cutting, grinding, polishing, and annealing. Although resonators of 1 kg and 150 mm diameter have been deemed feasible for metrology applications [38], we limit the crystal size to 25 mm diameter for initial production, as the strict tolerance requirements make the manufacturing of large SC-cut crystals challenging. In contrast, AT-cut resonators have less stringent requirements but still necessitate low-temperature characterization. Electrodes deposited on the disk surfaces provide a simple and effective solution for signal pick-up, although alternative packages are also under investigation. The results of these developments will be discussed in future publications. The primary objective is to achieve high-quality factors in large crystals at low overtones, chiefly for the mode $\lambda = \{A, 1, 0, 0\}$, which holds the promise of the highest sensitivity to gravitational waves for quartz BAWs. The envelope of the projected peak strain sensitivities of an array of two sets of eight BAWs of these dimensions is shown in Figure 1, where a fivefold gain on the current sensitivity is anticipated from performance optimizations at low overtones and the increase in the detector mass, including resonator diameter and total quantity.

Author Contributions: Conceptualization, T.T.d.F.; methodology, software, and validation, G.A., M.B., L.C., R.C., F.D.G., M.F., E.F., R.G., A.G. (Alessio Ghezzi), A.G. (Andrea Giachero), C.G., L.M., A.N., G.P., and D.R.; formal analysis, M.B., L.C., D.L., and L.M.; investigation, M.B., L.C., F.D.G., E.F., R.G., L.M., and D.R.; resources, M.F., E.F., C.G., A.N., G.P., and D.R.; data curation, M.B., L.C., F.D.G., R.G., and L.M.; writing—original draft preparation, T.T.d.F.; writing—review and editing, M.B., L.C., D.L., L.M., and T.T.d.F.; visualization, T.T.d.F.; supervision, T.T.d.F.; project administration, L.C. and T.T.d.F.; funding acquisition, T.T.d.F. All authors have read and agreed to the published version of the manuscript.

Funding: This research received funding from the Italian Ministry for Universities and Research (MUR) under grant "Dipartimenti di Eccellenza 2023-2027" and the PNRR MUR Project under grant PE0000023-NQSTI.

Institutional Review Board Statement: Not applicable.

Data Availability Statement: The raw data supporting the conclusions of this article will be made available by the authors upon request.

Acknowledgments: This research is developed within the framework of the "*Centro Bicocca di Cosmologia Quantitativa*" (BiCoQ), supported by the Italian Ministry for Universities and Research (MUR) under Grant "*Dipartimenti di Eccellenza 2023-2027*". The PNRR MUR Project also provided support to this work under grant PE0000023-NQSTI. We are indebted and sincerely grateful to Mike Tobar, Maxim Goryachev, and William Campbell for their assistance and guidance in launching this activity. We thank Mauro Fasoli and Chiara Liliana Boldrini, from the Department of Materials Sciences at the University of Milano Bicocca, for the geometry, roughness, and crystal properties measurements of the 'sacrificed' BAW sample.

Conflicts of Interest: The authors declare no conflicts of interest. The funders had no role in the design of the study; in the collection, analysis, or interpretation of data; in the writing of the manuscript; or in the decision to publish the results.

Abbreviations

The following abbreviations are used in this manuscript:

BAW	Bulk acoustic wave
GW	Gravitational wave
FLL	Flux locked loop
FPGA	Field programmable gate array
HFGW	High-frequency gravitational wave
Q	Quality factor
QCD	Quantum chromodynamics
SQUID	Superconducting quantum interference device
VNA	Vector network analyzer

Notes

[1] Magnicon, Niobium-based 2-stage SQUID current sensor chip, with XXF-1-20 DC-SQUID electronics.
[2] Xilinx Zynq UltraScale+ FPGA RFSoC4x2, which supports four 14-bit 4.096 Gsample/s ADCs.
[3] Rakon 5.175MHz SC P3 HC40/T2108.

References

1. Abbott, B.P.; Abbott, R.; Abbott, T.D.; Abernathy, M.R.; Acernese, F.; Ackley, K.; Adams, C.; Adams, T.; Addesso, P.; Adhikari, R.X.; et al. Observation of Gravitational Waves from a Binary Black Hole Merger. *Phys. Rev. Lett.* **2016**, *116*, 061102. [CrossRef]
2. The LIGO Scientific Collaboration and The Virgo Collaboration; The 1M2H Collaboration; The Dark Energy Camera GW-EM Collaboration and the DES Collaboration; The DLT40 Collaboration; The Las Cumbres Observatory Collaboration; The VINROUGE Collaboration; The MASTER Collaboration. A gravitational-wave standard siren measurement of the Hubble constant. *Nature* **2017**, *551*, 85–88. [CrossRef]
3. Moore, C.J.; Cole, R.H.; Berry, C.P.L. Gravitational-wave sensitivity curves. *Class. Quantum Gravity* **2014**, *32*, 015014. [CrossRef]
4. Aggarwal, N.; Aguiar, O.D.; Bauswein, A.; Cella, G.; Clesse, S.; Cruise, A.M.; Domcke, V.; Figueroa, D.G.; Geraci, A.; Goryachev, M.; et al. Challenges and opportunities of gravitational-wave searches at MHz to GHz frequencies. *Living Rev. Relativ.* **2021**, *24*, 4. [CrossRef]
5. Franciolini, G.; Maharana, A.; Muia, F. Hunt for light primordial black hole dark matter with ultrahigh-frequency gravitational waves. *Phys. Rev. D* **2022**, *106*, 103520. [CrossRef]
6. Arvanitaki, A.; Dubovsky, S. Exploring the string axiverse with precision black hole physics. *Phys. Rev. D* **2011**, *83*, 044026. [CrossRef]
7. Casalderrey-Solana, J.; Mateos, D.; Sanchez-Garitaonandia, M. Mega-Hertz Gravitational Waves from Neutron Star Mergers. *arXiv* **2022**, arXiv:2210.03171. [CrossRef]
8. Cruise, A.M.; Ingley, R.M.J. A prototype gravitational wave detector for 100 MHz. *Class. Quantum Gravity* **2006**, *23*, 6185. [CrossRef]
9. Cruise, A.M. The potential for very high-frequency gravitational wave detection. *Class. Quantum Gravity* **2012**, *29*, 095003. [CrossRef]
10. Nishizawa, A.; Kawamura, S.; Akutsu, T.; Arai, K.; Yamamoto, K.; Tatsumi, D.; Nishida, E.; Sakagami, M.A.; Chiba, T.; Takahashi, R.; et al. Laser-interferometric detectors for gravitational wave backgrounds at 100 MHz: Detector design and sensitivity. *Phys. Rev. D* **2008**, *77*, 022002. [CrossRef]
11. Akutsu, T.; Kawamura, S.; Nishizawa, A.; Arai, K.; Yamamoto, K.; Tatsumi, D.; Nagano, S.; Nishida, E.; Chiba, T.; Takahashi, R.; et al. Search for a Stochastic Background of 100-MHz Gravitational Waves with Laser Interferometers. *Phys. Rev. Lett.* **2008**, *101*, 101101. [CrossRef]
12. Chou, A.S.; Gustafson, R.; Hogan, C.; Kamai, B.; Kwon, O.; Lanza, R.; Larson, S.L.; McCuller, L.; Meyer, S.S.; Richardson, J.; et al. MHz gravitational wave constraints with decameter Michelson interferometers. *Phys. Rev. D* **2017**, *95*, 063002. [CrossRef]
13. Ejlli, A.; Ejlli, D.; Cruise, A.M.; Pisano, G.; Grote, H. Upper limits on the amplitude of ultra-high-frequency gravitational waves from graviton to photon conversion. *Eur. Phys. J. C* **2019**, *79*, 1032. [CrossRef]
14. Fujita, T.; Kamada, K.; Nakai, Y. Gravitational waves from primordial magnetic fields via photon-graviton conversion. *Phys. Rev. D* **2020**, *102*, 103501. [CrossRef]
15. Ito, A.; Ikeda, T.; Miuchi, K.; Soda, J. Probing GHz gravitational waves with graviton–magnon resonance. *Eur. Phys. J. C* **2020**, *80*, 179. [CrossRef]

16. Herman, N.; Fűzfa, A.; Lehoucq, L.; Clesse, S. Detecting planetary-mass primordial black holes with resonant electromagnetic gravitational-wave detectors. *Phys. Rev. D* **2021**, *104*, 023524. [CrossRef]
17. Tobar, M.E.; Thomson, C.A.; Campbell, W.M.; Quiskamp, A.; Bourhill, J.F.; McAllister, B.T.; Ivanov, E.N.; Goryachev, M. Comparing Instrument Spectral Sensitivity of Dissimilar Electromagnetic Haloscopes to Axion Dark Matter and High Frequency Gravitational Waves. *Symmetry* **2022**, *14*, 2165. [CrossRef]
18. Domcke, V.; Garcia-Cely, C.; Rodd, N.L. Novel Search for High-Frequency Gravitational Waves with Low-Mass Axion Haloscopes. *Phys. Rev. Lett.* **2022**, *129*, 041101. [CrossRef]
19. Gatti, C.; Visinelli, L.; Zantedeschi, M. Cavity detection of gravitational waves: Where do we stand? *Phys. Rev. D* **2024**, *110*, 023018. [CrossRef]
20. Gao, Y.; Xu, W.; Zhang, H. A Mössbauer scheme to probe gravitational waves. *Sci. Bull.* **2024**, *69*, 2795–2798. [CrossRef]
21. Domcke, V.; Ellis, S.A.R.; Rodd, N.L. Magnets are Weber Bar Gravitational Wave Detectors. *arXiv* **2024**, arXiv:2408.01483. [CrossRef]
22. Arvanitaki, A.; Geraci, A.A. Detecting High-Frequency Gravitational Waves with Optically Levitated Sensors. *Phys. Rev. Lett.* **2013**, *110*, 071105. [CrossRef]
23. Goryachev, M.; Tobar, M.E. Gravitational wave detection with high-frequency phonon trapping acoustic cavities. *Phys. Rev. D* **2014**, *90*, 102005. Erratum in: *Phys. Rev. D* **2023**, *108*, 129901. [CrossRef]
24. Tobar, G.; Pikovski, I.; Tobar, M.E. Detecting kHz gravitons from a neutron star merger with a multi-mode resonant mass detector. *arXiv* **2024**, arXiv:2406.16898. [CrossRef]
25. Goryachev, M.; Campbell, W.M.; Heng, I.S.; Galliou, S.; Ivanov, E.N.; Tobar, M.E. Rare Events Detected with a Bulk Acoustic Wave High Frequency Gravitational Wave Antenna. *Phys. Rev. Lett.* **2021**, *127*, 071102. [CrossRef] [PubMed]
26. Campbell, W.; Goryachev, M.; Tobar, M.E. The Multi-mode Acoustic Gravitational Wave Experiment: MAGE. *Sci. Rep.* **2023**, *13*, 10638. [CrossRef]
27. Besson, R. A New "Electrodeless" Resonator Design. In Proceedings of the 31st Annual Symposium on Frequency Control, Atlantic City, NJ, USA, 1–3 June 1977; pp. 147–152. [CrossRef]
28. Arvanitaki, A.; Dimopoulos, S.; Van Tilburg, K. Sound of Dark Matter: Searching for Light Scalars with Resonant-Mass Detectors. *Phys. Rev. Lett.* **2016**, *116*, 031102. [CrossRef]
29. Manley, J.; Wilson, D.J.; Stump, R.; Grin, D.; Singh, S. Searching for Scalar Dark Matter with Compact Mechanical Resonators. *Phys. Rev. Lett.* **2020**, *124*, 151301. [CrossRef]
30. Trickle, T. Piezoelectric Bulk Acoustic Resonators For Dark Photon Detection. *arXiv* **2025**, arXiv:2501.05504. [CrossRef]
31. Schmitt, R.F.; Allen, J.W.; Vetelino, J.F.; Parks, J.; Zhang, C. Bulk acoustic wave modes in quartz for sensing measurand-induced mechanical and electrical property changes. *Sens. Actuators B Chem.* **2001**, *76*, 95–102. [CrossRef]
32. EerNisse, E. Quartz Resonator Frequency Shifts Arising from Electrode Stress. In Proceedings of the 29th Annual Symposium on Frequency Control, Atlantic City, NJ, USA, 28–30 May 1975; pp. 1–4. [CrossRef]
33. Stevens, D.; Tiesten, H. An Analysis of doubly rotated quartz resonators utilizing essentially thickness modes with transverse variation. *J. Acoust. Soc. Am.* **1986**, *79*, 1811–1826. [CrossRef]
34. Galliou, S.; Goryachev, M.; Bourquin, R.; Abbé, P.; Aubry, J.P.; Tobar, M.E. Extremely Low Loss Phonon-Trapping Cryogenic Acoustic Cavities for Future Physical Experiments. *Sci. Rep.* **2012**, *3*, 2132. [CrossRef] [PubMed]
35. Goryachev, M.; Ivanov, E.N.; van Kann, F.; Galliou, S.; Tobar, M.E. Observation of the fundamental Nyquist noise limit in an ultra-high Q-factor cryogenic bulk acoustic wave cavity. *Appl. Phys. Lett.* **2014**, *105*, 153505. [CrossRef]
36. Campbell, W.M.; Mariani, L.; Parashar, S.; Tobar, M.E.; Goryachev, M. Low Temperature Properties of Low-Loss Macroscopic Lithium Niobate Bulk Acoustic Wave Resonators. *arXiv* **2025**, arXiv:2407.17693. [CrossRef]
37. Goryainov, S.V. Algorithm of the selection of materials for detector of high-frequency gravitational waves. *Eur. Phys. J. Plus* **2023**, *138*, 222. [CrossRef]
38. Vig, J.; Howe, D. A one-kilogram quartz resonator as a mass standard. *IEEE Trans. Ultrason. Ferroelectr. Freq. Control* **2013**, *60*, 428–431. [CrossRef] [PubMed]